HHS Public Access

Author manuscript

J Mol Biol. Author manuscript; available in PMC 2022 June 25.

Published in final edited form as:

J Mol Biol. 2021 June 25; 433(13): 166963. doi:10.1016/j.jmb.2021.166963.

The ER chaperones BiP and Grp94 regulate the formation of insulin-like growth factor 2 (IGF2) oligomers.

Yi Jin[1], **Judy L.M. Kotler**[1], **Shiyu Wang**[2], **Bin Huang**[1], **Jackson C. Halpin**[1], **Timothy O. Street**[3]

[1]Department of Biochemistry, Brandeis University, Waltham, MA 02454, USA

[2]Department of Biology, Brandeis University, Waltham, MA 02454, USA

[3]Department of Biochemistry, Brandeis University, Waltham, MA 02454, USA.

Abstract

While cytosolic Hsp90 chaperones have been extensively studied, less is known about how the ER Hsp90 paralog Grp94 recognizes clients and influences client folding. Here, we examine how Grp94 and the ER Hsp70 paralog, BiP, influence the folding of insulin-like growth factor 2 (IGF2), an established client protein of Grp94. ProIGF2 is composed of a disulfide-bonded insulin-like hormone and a C-terminal E-peptide that has sequence characteristics of an intrinsically disordered region. BiP and Grp94 have a minimal influence on folding whereby both chaperones slow proIGF2 folding and do not substantially alter the disulfide-bonded folding intermediates, suggesting that BiP and Grp94 may have an additional influence unrelated to proIGF2 folding. Indeed, we made the unexpected discovery that the E-peptide region allows proIGF2 to form dynamic oligomers. ProIGF2 oligomers can transition from a dynamic state that is capable of exchanging monomers to an irreversibly aggregated state, providing a plausible role for BiP and Grp94 in regulating proIGF2 oligomerization. In contrast to the modest influence on folding, BiP and Grp94 have a stronger influence on proIGF2 oligomerization and these chaperones exert counteracting effects. BiP suppresses proIGF2 oligomerization while Grp94 can enhance proIGF2 oligomerization in a nucleotide-dependent manner. We propose that BiP and Grp94 regulate the assembly and dynamic behavior of proIGF2 oligomers, although the biological role of proIGF2 oligomerization is not yet known.

Graphical Abstract

tstreet@brandeis.edu.

CRediT Author Statement

Yi Jin: Conceptualization, Methodology, Validation, Formal analysis, Software, Investigation, Writing-Original Draft, Writing-Review & Editing, Visualization, Project administration.

Judy L.M. Kotler: Investigation, Formal Analysis.

Shiyu Wang & Bin Huang: Investigation.

Jackson C. Halpin: Methodology.

Timothy O. Street: Conceptualization, Software, Writing- Review & Editing, Project administration, Supervision, Funding acquisition.

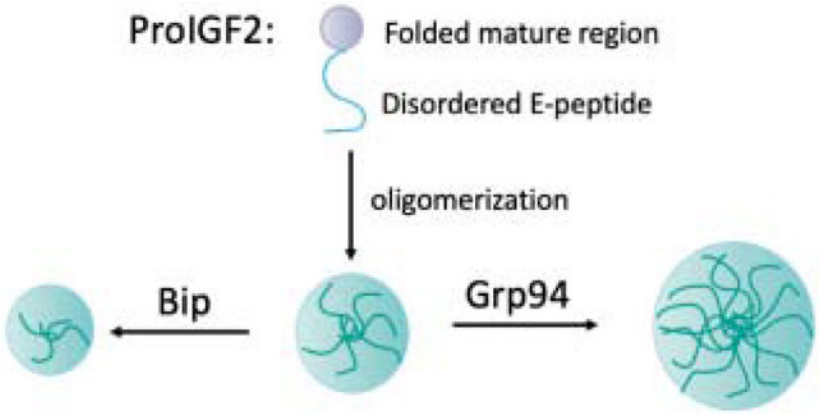

Introduction

Hsp70 and Hsp90 chaperones maintain protein quality control in the cytosol, while the endoplasmic reticulum (ER) and mitochondria have their own homologous Hsp70/Hsp90 systems (ER: BiP/Grp94, mitochondria: Mortalin/Trap1). Hsp70 and Hsp90 family members require ATP binding and hydrolysis to cycle through distinct conformational states with distinct client binding properties[1–7]. Both chaperones are heavily regulated by co-chaperones and post-translational modifications[8, 9]. Adding to this complexity, Hsp70 and Hsp90 often associate during the chaperoning process, which can make their functions interconnected[10, 11].

Client interactions with cytosolic Hsp90 have been extensively studied with recent advances in structural analysis by electron microscopy, NMR, and FRET[6, 12–16], however less is known about how Grp94 recognizes clients and subsequently influences their folding and activity. For example, while cytosolic Hsp90 can bind to clients in monomeric and oligomeric states[12–14, 17], it is not clear whether Grp94 operates in a similar manner. It is also unknown whether Grp94 stabilizes fully unfolded states or whether it can actively influence client folding. Here we examine interactions between Grp94, BiP, and IGF2. IGF2 is one of a small collection of ER proteins whose *in-vivo* stability is stringently dependent on Grp94[18]. Indeed, Grp94 is involved in the successful secretion of all members of the IGF family (insulin, IGF1 and IGF2)[19–22], but the underlying mechanism is not understood. Grp94 mutations that abolish ATP binding and hydrolysis cannot support cell viability in serum-free media due to the loss of secreted IGF2[20, 21]. In contrast to the limited clientele of Grp94, BiP exhibits broad specificity due to the ubiquity of the short hydrophobic motifs that it recognizes[23].

IGF proteins have three disulfide bonds in the hormone region. Disulfide-bonded proteins are well-suited for studying folding pathways because their folding intermediates can be trapped by quenching techniques and separated by reverse-phase HPLC (RP-HPLC). These methods have been applied with success to robust folding systems, like bovine pancreatic trypsin inhibitor (BPTI)[24, 25], but little is known about whether the same set of techniques can reveal the folding properties of proteins that are in the process of receiving chaperone assistance.

Mouse IGF2 is composed of a 24-residue signal sequence followed by a 67-residue hormone region and an 87-residue E-peptide region[26] (Figure 1A). Upon folding in the ER, proIGF2 is packaged into vesicles for transport to the Golgi[27] where proIGF2 is proteolytically separated into mature IGF2 (mIGF2) and the E-peptide[28]. *In-vitro* folding studies of IGF1 and IGF2 have focused on the mature constructs[29–31]. Here we focus on full-length proIGF2 because it is the biologically relevant construct for BiP and Grp94.

Little is known about the biological role of the E-peptide region, although it is predicted to be intrinsically disordered based on primary sequence (Figure 1A). Intrinsically disordered proteins (IDPs) have a strong propensity to form condensates[32–34], which are dynamic soluble oligomers that can transition into irreversible aggregates. Chaperones are believed to be involved in maintaining the dynamics and solubility of condensates[35, 36], however this is an active area of research with many open questions. Here we find that the E-peptide region promotes proIGF2 oligomerization, and that Grp94 and BiP exert counteracting effects on the growth of proIGF2 oligomers.

Results

Under denaturing conditions proIGF2 can be fully reduced by TCEP (Figure 1C) and subsequent experiments are initiated by diluting proIGF2 out of denaturant. After dilution proIGF2 maintains a fully reduced state under TCEP conditions, whereas proIGF2 folds under oxidizing conditions using a mixture of oxidized and reduced glutathione. Figure 1B shows how proIGF2 folding can be monitored by RP-HPLC (see Methods for details). Folding and disulfide formation are quenched by phosphoric acid. The quenched samples remain soluble and do not change their disulfide status for at least 20h (Supplemental Figure 1A). A commercial standard of mIGF2 has a similar retention time as the major population of the recombinant refolded mIGF2 (Supplemental Figure 1B), indicating that proper refolding has occurred.

ProIGF2 folding kinetics are pH-dependent and influenced by the solution reduction potential (Supplemental Figure 1C and 1D). We selected pH 7.5 and a reduction potential of 5.0 (ratio of [GSH]/[GSSG][37]) for more detailed analysis of proIGF2 folding. Under these conditions proIGF2 undergoes a modest level of misfolding and aggregation. For example, after 30 minutes of folding under these conditions the soluble fraction of proIGF2 is 72±7% of the starting material. Thus, these conditions allow for potential improvements in proIGF2 folding to be observed from the influence of BiP and Grp94.

Multiple folding states of proIGF2 and mIGF2 are populated during refolding (Figure 1C, Supplemental Figure 1B). A complete folding analysis is not feasible due to overlapping chromatography peaks, which also precludes a more complex description of proIGF2 folding that includes off-pathway intermediates and misfolded states. However, a simplified folding description can be achieved by combining elution peaks into three groups based on their retention times (Figure 1D and Supplemental Figure 1E, see Methods for details). We find that proIGF2 and mIGF2 follow similar folding kinetics (Figure 1E and Supplemental Figure 1F), indicating that the E-peptide region does not have a strong influence on the folding of the mature region.

BiP and Grp94 have only a modest influence on proIGF2 folding

BiP and Grp94 ATPase activity are both increased by proIGF2 (Supplemental Figure 2), indicating that the chaperones indeed interact with proIGF2. However, BiP and Grp94 could influence proIGF2 folding through a wide variety of mechanisms. For example, BiP and Grp94 could accelerate proIGF2 folding, selectively bind specific vulnerable folding intermediates, or even change the folding pathway to avoid vulnerable folding intermediates. The well-populated proIGF2 folding intermediates provide an opportunity to distinguish between these scenarios.

BiP, and to a lesser extent Grp94, decelerate proIGF2 folding (Figure 2A). BiP and Grp94 stabilize the proIGF2 unfolded state (11.6 minutes retention time) as is evident by its increased population (see 0.5 min folding time). The accumulation of proIGF2 folding intermediates is decelerated, for example the intermediate at 11.2 minutes retention time (see 1 min refolding time). Finally, the build-up of fully oxidized proIGF2 at 10.1 minutes retention time is also decelerated (see 2 min refolding time). No new highly populated folding intermediates are observed. A three-state kinetic analysis, like that performed for proIGF2 folding alone (Figure 1E), shows that BiP and Grp94 slow folding (Figure 2B, 2C), although for Grp94 the change is within the experimental error from replicate experiments. Similar to the modest influence of BiP and Grp94 on proIGF2 folding kinetics, these chaperones also have a minimal influence on the yield of soluble proIGF2 (Supplemental Figure 3). One final feature of proIGF2 folding is noteworthy. At long refolding times some of the proIGF2 does not convert to the native state, resulting in a distribution of folding states rather than a single uniform peak. This heterogeneity, which could be due to a population of terminally misfolded states, is also evident when BiP and Grp94 are present suggesting that these chaperones do not enable misfolded proIGF2 to refold properly.

Given the modest influence of and BiP and Grp94 on proIGF2 folding we questioned whether these chaperones may have an additional influence that is unrelated to proIGF2 folding. Indeed, much of the proIGF2 E-peptide is predicted to be disordered (Figure 1A). As described next, the E-peptide drives proIGF2 oligomerization, and BiP and Grp94 influence oligomerization in opposite ways.

ProIGF2 forms oligomers

Under reducing conditions unfolded proIGF2 scatters light, whereas neither the mIGF2 nor the E-peptide region alone scatters light (Figure 3A and Supplemental Figure 4A). Thus, it is the combination of the mIGF2-region and the intrinsically disordered E-peptide region that drives proIGF2 self-assembly.

The light-scattering from proIGF2 oligomerization does not have a lag-phase (Figure 3A), indicating that the self-association does not follow fibril-like kinetics in which rapid growth only occurs after a nucleus is formed. Similarly, proIGF2 self-association as measured by fluorescence depolarization also does not show evidence of strong cooperativity (Figure 3B), also similar to the behavior of condensates[38]. Dynamic light scattering (DLS) was used to determine the average hydrodynamic radius (R_H) of proIGF2 oligomers. At early time points

with 2μM proIGF2, these oligomers have a R_H of 230nm, and this size increases to 747nm after one hour (Table 1).

Fluorescently labeled proIGF2 oligomers can be visualized by confocal fluorescence microscopy (Figure 3C), both in solution and on the microscope slide. These oligomers have a circular appearance, although irregular shapes are observed at high proIGF2 concentration (see 10μM condition in Figure 3C). Because proIGF2 oligomers can be observed on the slide surface, we tested whether TIRF microscopy could be used to examine the oligomers on more detailed level. The TIRF measurements were conducted by forming proIGF2 oligomers at 2.5μM and then diluting proIGF2 to 25nM to achieve sparse coverage on the microscope slide. Under these conditions, proIGF2 oligomers of different sizes are visually apparent (Supplemental Figure 4C) and can be further illustrated by observing a variable number of stepwise fluorescence decreases over time (Supplemental Figure 4D). Quantification of proIGF2 oligomer fluorescence intensity suggests that proIGF2 oligomers have an approximately exponential size distribution rather than forming one specific size (Supplemental Figure 4E).

Given the critical role of the E-peptide in the formation proIGF2 oligomers, we sought to further characterize this region of proIGF2. Consistent with the sequence disorder prediction in Figure 1A, the E-peptide on its own has minimal secondary structure as measured by circular dichroism (Supplemental Figure 4B). The E-peptide by itself can undergo self-association as measured by fluorescence anisotropy (Figure 3B, inset), which suggests that the oligomerization is driven by weak interactions spread across a largely unstructured E-peptide. Both the E-peptide and proIGF2 oligomers can be disrupted by urea to a yield a lower polarization value (arrows, Figure 3B).

Closer inspection of the E-peptide sequence reveals a notable statistical enrichment of arginine residues (the 87 residue E-peptide contains 13 arginine residues) when compared against a database of folded proteins and disordered proteins (Figure 3D), while no such enrichment is observed for lysine[39]. A high relative abundance of arginine relative to lysine is a characteristic sequence feature that is often found in proteins that exhibit self-association[40], and for protein condensates pi-cation interactions between arginine and aromatic residues are an important driving force[41]. The only other statistically significant sequence feature of the E-peptide is a high proline content compared to well-folded proteins, consistent with the lack of a well-defined E-peptide structure.

BiP and Grp94 have opposing effects on proIGF2 oligomerization

BiP and Grp94 influence proIGF2 oligomerization in very different ways. Under both ADP and ATP conditions BiP suppresses proIGF2 oligomerization (Figure 4A), whereas under ADP conditions Grp94 enhances proIGF2 oligomerization (Figure 4B, Supplemental Figure 5). Interestingly, Grp94 enhances the magnitude of proIGF2 light-scattering but not the overall kinetics. Neither BiP nor Grp94 produce light scattering on their own (Figure 4A, B). Similar to the optical light scattering, DLS shows Grp94 increasing the R_H of ProIGF2 oligomers whereas BiP reduces their size (Table 1). These measurements show BiP decreasing the size of proIGF2 oligomers over time, suggesting that BiP can disassemble proIGF2 oligomers.

The above experiments were performed under reducing conditions in which the mature region of proIGF2 cannot fold. Under folding conditions proIGF2 exhibits a lower level of light-scattering, but even under these conditions Grp94 enhances proIGF2 oligomerization (Supplemental Figure 6A). Finally, we performed one further experimental variation in which proIGF2 is first allowed to completely oxidize, and then Grp94 is introduced, and hereto we also observe that Grp94 enhances proIGF2 oligomerization (Supplemental Figure 6B). These observations indicate that Grp94 promotes proIGF2 oligomerization under a wide variety of folding conditions.

The increased proIGF2 light scattering from Grp94 (Figure 4B) could be explained either by Grp94 enabling proIGF2 oligomers to increase their monomer copy number or alternatively by multiple Grp94 chaperones binding to proIGF2 oligomers and thus increasing the combined particle size. We used FRET to distinguish between these possibilities. We labeled proIGF2 with either a donor or acceptor fluorophore (see Methods). By mixing these separately labeled samples, proIGF2 oligomerization can be monitored by increasing FRET without any signal interference from Grp94 (Figure 4C). Grp94 enhances proIGF2 oligomerization FRET (Figure 4D) under ADP conditions indicating that Grp94 enables proIGF2 oligomers to increase their monomer copy number. Similar to the light-scattering measurements, we find that Grp94 enhances the extent of proIGF2 oligomerization with a minimal influence on the overall kinetics (Figure 4D).

Interestingly, the above FRET assay demonstrates that proIGF2 slowly transitions from dynamic oligomers to irreversible aggregates. The change in proIG2 oligomer dynamics can be observed by introducing Grp94 to proIGF2 oligomers at different times (Figure 5A). If proIGF2 can maintain a dynamic oligomerization state, then adding Grp94 at an earlier and later time would result in the same increase in FRET. In contrast, if proIGF2 oligomers transition to an irreversible aggregate then adding Grp94 at a later time would result in smaller increase in FRET. We observe this latter case, whereby Grp94-induced enhancement of proIGF2 FRET decreases over time (Figure 5B). Grp94 does not co-aggregate with proIGF2, as we find that the soluble concentration of Grp94 stays constant even as the soluble concentration of proIGF2 decreases (Supplemental Figure 7). We conclude that dynamic oligomers of proIGF2 slowly transform to irreversible rigid aggregates.

Collectively, the above measurements are consistent with Grp94 accelerating proIGF2 oligomerization. Figure 5C presents a minimal quantitative model for proIGF2 oligomerization and aggregation. Monomers of proIGF2 are added with a rate of k_+ and oligomers of any size can transition to an irreversibly aggregated state with a rate of k_A. The final average size of proIGF2 particles is given by k_+/k_A (we denote this ratio as R). This model yields proIGF2 oligomer and aggregate sizes that are exponentially distributed, consistent with the size distribution observed by TIRF microscopy (Supplemental Figure 4E). For example, Figure 5C shows the distribution of proIGF2 particle sizes in which the aggregation rate is set to 0.05 min^{-1} (similar to the aggregation kinetics measured in Figure 4) and the rate of monomer addition is arbitrarily set to 3.0 min^{-1}. The resulting particle sizes are exponentially distributed (sold line, Figure 5C), with average size (<n>=60) that is in line with the expected value (k_+/k_A=60). This model of oligomer growth does not yield a

lag-phase (Figure 5D), consistent with the light-scattering and FRET measurements in Figure 4D.

According to the model above, Grp94 can enhance proIGF2 oligomerization either by slowing the aggregation transition (decreasing k_A) or by accelerating oligomerization (increasing k_+). Because the light-scattering and FRET both show Grp94 enhancing the magnitude of oligomer formation but not the overall kinetics, this implies that Grp94 has a minimal influence on k_A but rather accelerates proIGF2 oligomerization dynamics (Grp94 increases k_+). Figure 5D shows an example numerical simulation of the influence of Grp94 on proIGF2 oligomerization in which Grp94 enhances proIGF2 oligomerization dynamics six-fold. In these numerical simulations Grp94 is introduced at various times during the course of proIGF2 oligomer formation, thus matching the design of the FRET experiments in Figure 5B. The numerical simulations and experimental data are in qualitative agreement (compare Figure 5B and Figure 5E). We conclude that the simple model in Figure 5C provides an adequate explanation of the influence of Grp94 on proIGF2 oligomerization.

Discussion

Here we examined how the BiP and Grp94 chaperones influence both the folding and the oligomerization of proIGF2 (Figure 6). One motivation for studying proIGF2 was to test the idea that Hsp90-family chaperones are specialized for the late stages of protein folding. Although prevalent in the Hsp90 literature[15, 42, 43] testing this concept has led to diverging results (*e.g.,* separate studies of p53 have found that client is folded, molten globule, and fully unfolded when bound to Hsp90[44–46]).

An empowering feature of IGF2 is that its disulfide-bonded folding intermediates can be trapped and separated by RP-HPLC similar to classic studies that uncovered the detailed folding pathways of BPTI[24, 25]. If Grp94 indeed strongly stabilizes specific folding states of IGF2, this experimental system would be able to detect which state is stabilized and quantify the extent of stabilization. However, we find that both BiP and Grp94 have only a modest influence on the folding properties of proIGF2 (Figures 1&2). Thus, for the proIGF2 client we do not see evidence that Grp94 is specialized for the later stages of client folding. An alternative mechanism may explain the sequential involvement of BiP and Grp94 with early and late stages of client folding, as has been observed for immunoglobins[47]. Specifically, the sequential involvement of BiP and Grp94 in client folding may arise simply from regulated direct interactions between BiP and Grp94, in which the conformation of BiP controls when Grp94 can access the client protein[48]. A further possibility is to examine the influence of BiP and Grp94 in an expanded chaperone system that includes a BiP nucleotide exchange factor and a J-protein co-chaperone. Future studies are needed to test this possibility.

In studying the folding properties of proIGF2 and mature IGF2, we discovered that the E-peptide region of proIGF2 promotes oligomerization (Figure 3). The high arginine content of the E-peptide (Figure 3D) may play a role in the oligomerization, possibly through cation-π interactions, as has been observed in other disordered oligomers[41]. Indeed, the role of the intrinsically disordered E-peptide region in promoting oligomerization is in-line with observations from the field of protein condensates[35, 49–52]. However, while *in-vitro* protein

condensates are typically in the range of 10 μm in size, proIGF2 oligomers are smaller (R_H ~200 nm).

Many peptide hormones, including insulin, oligomerize to promote efficient sorting in the secretory pathway[53–56]. ProIGF2 oligomerization has a plausible biological role in concentrating the pro-hormone into clusters that can be effectively packaged for transporting to the Golgi via COPII vesicles (Figure 6A). Because the E-peptide is cleaved off in the Golgi[28], the oligomerization property could be relevant to proIGF2 sorting at the ER-to-Golgi transition rather than for proIGF2 folding in the ER. Indeed, we find that the E-peptide has a minimal consequence on the folding of the mature region (Figure 1 and Supplemental Figure 1).

While BiP and Grp94 have a similar influence on proIGF2 folding, these chaperones have opposing effects on proIGF2 oligomerization (Figure 6B). BiP suppresses oligomerization while Grp94 enhances oligomerization both when the mature region of proIGF2 is unfolded (Figure 4) and folded (Supplemental Figure 6). Our findings with Grp94 and proIGF2 are consistent with reports that Grp94 enhances the self-association of the secreted protein myocilin[57]. We find that Grp94 enhances proIGF2 oligomerization by increasing the assembly rate (k_+ in Figure 5) rather than from slowing the transition into irreversible aggregates. Similar to Grp94, cytosolic human Hsp90β promotes the oligomerization of the intrinsically disordered protein tau via exposing its aggregation-prone repeat domain[58]. One proposed yet unverified function of chaperones on protein condensates is a role in increasing condensate dynamics as a mechanism to reduce irreversible aggregation process[49]. This idea is in line with our observation that proIGF2 undergoes a slow transition from dynamic oligomers to irreversible aggregates and that Grp94 can only act on the dynamic oligomers (Figure 5B). More work is needed to explore the biological consequences of the Grp94 influence on ProIGF2 oligomerization and some of these possibilities are listed in Figure 6B.

Grp94 enhances proIGF2 oligomerization when Grp94 adopts the open state (ADP conditions) but not under ATP conditions where Grp94 cycles between the open and closed states[59] (Figure 3A,B), which suggests that the open and closed conformations have opposing effects on proIGF2 oligomerization. Future work is needed to determine how the open state of Grp94 accelerates proIGF2 oligomerization. The Grp94 open state, as with the open state of all Hsp90 chaperones, is conformationally heterogeneous[60–62]. One possibility is that this conformational heterogeneity may help Grp94 interact with the heterogeneous environment of a proIGF2 oligomer.

Material and Methods

Protein expression and purification

Mouse proIGF2, mIGF2 and E-peptide were purified from *Escherichia coli* BL21* cells. Cells were grown at 37°C in LB medium and induced at OD_{600}=0.6~0.8 with 0.1mM IPTG at 30°C overnight. ProIGF2 and mIGF2 proteins were purified through inclusion body extraction and ion exchange chromatography. Purified IGF2 constructs were stored in 8M urea, 100mM Tris pH7.5, 25mM KCl, 1mM EDTA, 1mM TCEP. Purified E-peptide was

stored in 8M urea, 25 mM Tris, pH 7.5, 250 mM KCl, 1 mM DTT. An additional poly-histidine tag on the E-peptide was removed via TEV protease and a Histrap column and stored in 25mM Tris pH 7.5, 150mM KCl, 50mM imidazole buffer.

The purification of mouse Grp94 without the charged linker (Δ287–328) and BiP is similar to previously described methods[63, 64]. Briefly, BiP and Grp94 were expressed in *Escherichia coli* strain BL21* at 37°C and purified via a Histrap column (GE Healthcare), ion-exchange column (MonoQ, GE Healthcare), and by gel filtration (Superdex S-20, GE Healthcare). Proteins were flash-frozen in 50mM Tris, pH7.5, 50mM KCl, 5mM $MgCl_2$ and 5% glycerol.

ATPase measurement

BiP and Grp94 ATPase was measured with a temperature-controlled plate reader (BioTeK) with an ATP-regenerating system at 37°C as previously described[65]. All experiments were performed with 50mM Tris, pH 7.5, 100mM KCl, 1mM ATP, 1mM $MgCl_2$, 5mM TCEP and 0.8M urea with 1.5μM BiP or 1.5μM Grp94 (dimer), and 5μM IGF2 constructs at 37 °C. ATPase activity was determined by NADH consumption rate measured at 340nm.

Reverse phase HPLC

To measure proIGF2/mIGF2 folding, samples were diluted 1:10 out of denaturant into refolding/reduced buffer (50mM Tris, pH 7.5, 100mM KCl, 6.25mM GSH, 1.25mM GSSG, or 5mM TCEP (reduced), 1mM ATP/ADP, 1mM $MgCl_2$) at 37°C. The final concentrations of proIGF2, BiP and Grp94 were all 5μM. At various time points, proIGF2 refolding reactions were quenched by 500mM H_3PO_4 and 5% acetonitrile. The quenched samples were spun down at 15,000g for 3min and the supernatant was injected to C4–300 reverse-phase column (ACE, 100 × 4.6mm, 5μm). Different proIGF2 folding states were separated with 50mM H_3PO_4 in H_2O (Buffer A) with a linear acetonitrile gradient with 50mM H_3PO_4 (Buffer B) and a flow rate of 1ml/min. ProIGF2 elution profiles were detected by absorbance at 220nm. To determine the populations of folding states for the three-state analysis (Figure 1E, Supplemental Figure 1F) the absorbance at 220nm was integrated for the U, I, and N regions and normalized to the total integrated area. The fitting of the three-state model is described in the Appendix.

Light scattering

IGF2 constructs were diluted to 5μM into a reducing buffer (50 mM Tris, pH 7.5, 100 mM KCl, 1 mM $MgCl_2$, 5 mM TCEP, 0.8 M urea, 1 mM ATP/ADP, 25°C) with or without a stochiometric concentration of BiP and Grp94. Light scattering signals were monitored by light absorption at 420 nm.

Dynamic light scattering

ProIGF2 hydrophobic radius (R_h) was measured with am ALV/DLS/SLS-5000 Compact Goniometer System at room temperature. ProIGF2 samples were diluted to 2μM into a reducing buffer (50mM Tris, pH 7.5, 100mM KCl, 1mM $MgCl_2$, 5mM TCEP, 0.8M urea, 1mM ADP, 25°C) with or without 5μM of BiP or Grp94. Samples were spun down at 20000 × g and the supernatant was monitored at a 90° angle by laser light scattering at 633nm. The translational diffusion coefficient was obtained by analyzing the autocorrelation fluctuation

and R_h is calculated from the diffusion coefficient. The samples containing chaperones and proIGF2 are polydisperse because R_H values of BiP and Grp94 are below 10nm (BiP: 3.0nm, Grp94 3.2nm). Thus, the mass-weight distribution (M_w) of particles with R_H<10nm was excluded to minimize the interference of the chaperones on proIGF2 oligomer size calculation[66].

Fluorescence polarization measurements

ProIGF2 was labeled with a 2-fold excess of fluorescein isothiocyanate (FITC) for 1hr under buffer conditions of 100 mM Tris pH 7.5, 25mM KCl, 1mM EDTA, 8M urea, at room temperature. The labeling reaction was quenched with 5mM 2-mercaptoethanol, and free dye was removed from labeled protein by ion-exchange chromatography. Protein was stored in 8M urea, 100 mM Tris pH 7.5, 500 mM KCl, 1 mM EDTA, 1 mM TCEP. Fluorescence polarization measurements were performed with 100nM labeled proIGF2 on a Fluoromax-4-spectrofluorometer (Horiba Scientific) with an excitation wavelength of 485nm and emission wavelength of 520 nm with 3nm slit width. Labeled proIGF2 was preincubated with proIGF2 in a matching 8 M urea buffer before measurements, and then diluted ten-fold into a reducing buffer (100 mM Tris pH 7.5, 100 mM KCl, 1 mM ATP, 1 mM $MgCl_2$, 1 mM TCEP, 0.8M urea) to measure the fluorescence polarization at 37°C. Fluorescence polarization measurements on the E-peptide were performed with 50 nM labeled E-peptide titrated in a reducing buffer (60 mM MES pH 6.0, 100 mM KCl, 1 mM $MgCl_2$, 1 mM ADP, 0.5 mg/mL BSA, 1 mM DTT).

Förster resonance energy transfer

ProIGF2 was labeled with a stochiometric concentration of AlexaFluor 555 C2 maleimide or AlexaFluor 647 C2 maleimide (Invitrogen) for 4hr at room temperature. Free dye was removed via an SP column. The labeling rate for both fluorophores was determined to be 20% by spectrophotometric measurements. ProIGF2 was stored in reduced denaturant buffer (100 mM Tris pH 7.5, 25 mM KCl, 1 mM EDTA, 1 mM TCEP, 8M urea). FRET measurements were initiated by mixing 250nM donor-labeled proIGF2, 250nM acceptor-labeled proIGF2 and 2μM unlabeled proIGF2. The mixture was diluted into 25mM Tris pH 7.5, 100mM KCl, 1mM ADP, 1mM $MgCl_2$, 5mM TCEP, 0.8M urea buffer. The FRET kinetics were monitored by exciting donor fluorophore at 532nm, and detecting donor and acceptor at 565nm and 670nm respectively, with slit width of 4nm and a time interval of 30s. The FRET efficiency was calculated as $E_{FRET} = I_{Acceptor}/(I_{Donor}+I_{Acceptor})$, where I_{donor} and $I_{acceptor}$ are the donor and acceptor emission intensities observed at donor and acceptor detection wavelengths.

Confocal microscopy

Alexa Fluoro-647 labeled proIGF2 was diluted to various concentrations in 50 mM Tris pH 7.5, 100 mM KCl, 1 mM ATP, 1 mM $MgCl_2$, 5 mM TCEP buffer. All proIGF2 oligomer images were obtained on an Observer Z1 microscope (Carl Zeiss) equipped with a CSU-X1 spinning-disk confocal head (Yoka-gawa) and a QuantEM 512SC EM charge-coupled device (CCD) camera (Photometrics) with a 100× (NA 1.45) oil-immersion-objective at room temperature. Confocal Z-stacks were collected every 15s for 5min, with manual focus adjustment. Fluorescence microscope image analysis was performed using ImageJ.

Total Internal Reflection Fluorescence Microscopy (TIRF)

Alexa Fluor-555 labeled proIGF2 was diluted from 2.5 μM to 25 nM into 50 mM Tris buffer (pH 7.5, 50 mM Tris 50 mM KCl, 600 μM $MgCl_2$, 0.5 mg/ml BSA, 600 μM ADP and equilibrated at room temperature. Glass slides, coverslips and sample preparation followed previously descriptions[67, 68]. Single molecule TIRF imaging of proIGF2 oligomers was performed on a custom microscope[69], using 532 nm excitation wavelength and a 2.4 s sampling interval with 600 μW laser power. Data analysis and spot identification was performed on custom software built in Matlab, available online (https://github.com/gelles-brandeis/CoSMoS_Analysis).

Numerical simulations

Numerical simulations in Figure 5 were performed in Python using Gillespie sampling. The k_A rate constant (0.05 min^{-1}) was determined from the light scattering kinetics in Figure 3. The k_+ rate 3 min^{-1} (without Grp94) and 18 min^{-1} with Grp94, were selected arbitrarily. Both oligomers and irreversible aggregations were included in calculating the average size of proIGF2 particles <n>, which represents the average number of proIGF2 monomers per particle.

Circular Dichroism

E-peptide was diluted 1:10 out of denaturant at 25°C. The final concentration of E-peptide in the experiment was 8.1 μM in 0.8 M urea, 2.5 mM Tris, 25 mM KCl, and 0.1 mM DTT. Measurements were performed on a Jasco J-810 Circular Dichroism System.

Supplementary Material

Refer to Web version on PubMed Central for supplementary material.

Acknowledgements

The authors would like to thank Gelles and Street lab members for helpful discussion and feedback. Research for this project was supported by NIH R01 GM115356 (T.O.S). Authors have no interest of conflict.

References

1. Shiau AK; Harris SF; Southworth DR; Agard DA, Structural Analysis of E Structural Analysis of E. coli hsp90 reveals dramatic nucleotide-dependent conformational rearrangements. Cell 2006, 127 (2), 329–40. [PubMed: 17055434]
2. Hessling M; Richter K; Buchner J, Dissection of the ATP-induced conformational cycle of the molecular chaperone Hsp90. Nature structural & molecular biology 2009, 16 (3), 287–93.
3. McCarty JS; Buchberger A; Reinstein J; Bukau B, The role of ATP in the functional cycle of the DnaK chaperone system. J Mol Biol 1995, 249 (1), 126–37. [PubMed: 7776367]
4. Kityk R; Kopp J; Sinning I; Mayer MP, Structure and dynamics of the ATP-bound open conformation of Hsp70 chaperones. Mol Cell 2012, 48 (6), 863–74. [PubMed: 23123194]
5. Arakawa A; Handa N; Shirouzu M; Yokoyama S, Biochemical and structural studies on the high affinity of Hsp70 for ADP. Protein Sci 2011, 20 (8), 1367–79. [PubMed: 21608060]
6. Schopf FH; Biebl MM; Buchner J, The HSP90 chaperone machinery. Nat Rev Mol Cell Biol 2017, 18 (6), 345–360. [PubMed: 28429788]

7. Rosenzweig R; Nillegoda NB; Mayer MP; Bukau B, The Hsp70 chaperone network. Nat Rev Mol Cell Biol 2019, 20 (11), 665–680. [PubMed: 31253954]
8. Li J; Soroka J; Buchner J, The Hsp90 chaperone machinery: conformational dynamics and regulation by co-chaperones. Biochim Biophys Acta 2012, 1823 (3), 624–35. [PubMed: 21951723]
9. Duncan EJ; Cheetham ME; Chapple JP; van der Spuy J, The role of HSP70 and its co-chaperones in protein misfolding, aggregation and disease. Subcell Biochem 2015, 78, 243–73. [PubMed: 25487025]
10. Genest O; Hoskins JR; Kravats AN; Doyle SM; Wickner S, Hsp70 and Hsp90 of E. coli Directly Interact for Collaboration in Protein Remodeling. Journal of molecular biology 2015, 427 (24), 3877–89. [PubMed: 26482100]
11. Kravats AN; Doyle SM; Hoskins JR; Genest O; Doody E; Wickner S, Interaction of E Interaction of E. coli Hsp90 with DnaK Involves the DnaJ Binding Region of DnaK. J Mol Biol 2016.
12. Daturpalli S; Waudby CA; Meehan S; Jackson SE, Hsp90 inhibits alpha-synuclein aggregation by interacting with soluble oligomers. J Mol Biol 2013, 425 (22), 4614–28. [PubMed: 23948507]
13. Karagoz GE; Duarte AM; Akoury E; Ippel H; Biernat J; Moran Luengo T; Radli M; Didenko T; Nordhues BA; Veprintsev DB; Dickey CA; Mandelkow E; Zweckstetter M; Boelens R; Madl T; Rudiger SG, Hsp90-Tau complex reveals molecular basis for specificity in chaperone action. Cell 2014, 156 (5), 963–74. [PubMed: 24581495]
14. Lackie RE; Maciejewski A; Ostapchenko VG; Marques-Lopes J; Choy WY; Duennwald ML; Prado VF; Prado MAM, The Hsp70/Hsp90 Chaperone Machinery in Neurodegenerative Diseases. Front Neurosci 2017, 11, 254. [PubMed: 28559789]
15. Radli M; Rudiger SGD, Dancing with the Diva: Hsp90-Client Interactions. J Mol Biol 2018, 430 (18 Pt B), 3029–3040. [PubMed: 29782836]
16. Verba KA; Wang RY-R; Arakawa A; Liu Y; Shirouzu M; Yokoyama S; Agard DA, Atomic structure of Hsp90-Cdc37-Cdk4 reveals that Hsp90 traps and stabilizes an unfolded kinase. Science (New York, N.Y.) 2016, 352 (6293), 1542–1547.
17. Shelton LB; Koren J 3rd; Blair LJ, Imbalances in the Hsp90 Chaperone Machinery: Implications for Tauopathies. Front Neurosci 2017, 11, 724. [PubMed: 29311797]
18. Argon Y; Bresson SE; Marzec MT; Grimberg A, Glucose-Regulated Protein 94 (GRP94): A Novel Regulator of Insulin-Like Growth Factor Production. Cells 2020, 9 (8).
19. Ghiasi SM; Dahlby T; Hede Andersen C; Haataja L; Petersen S; Omar-Hmeadi M; Yang M; Pihl C; Bresson SE; Khilji MS; Klindt K; Cheta O; Perone MJ; Tyrberg B; Prats C; Barg S; Tengholm A; Arvan P; Mandrup-Poulsen T; Marzec MT, Endoplasmic Reticulum Chaperone Glucose-Regulated Protein 94 Is Essential for Proinsulin Handling. Diabetes 2019, 68 (4), 747–760. [PubMed: 30670477]
20. Ostrovsky O; Ahmed NT; Argon Y; Brodsky JL, The Chaperone Activity of GRP94 Toward Insulin-like Growth Factor II Is Necessary for the Stress Response to Serum Deprivation. Molecular Biology of the Cell 2009, 20 (6), 1855–1864. [PubMed: 19158397]
21. Ostrovsky O; Makarewich CA; Snapp EL; Argon Y, An essential role for ATP binding and hydrolysis in the chaperone activity of GRP94 in cells. P Natl Acad Sci USA 2009, 106 (28), 11600–11605.
22. Ostrovsky O; Eletto D; Makarewich C; Barton ER; Argon Y, Glucose regulated protein 94 is required for muscle differentiation through its control of the autocrine production of insulin-like growth factors. Biochimica et biophysica acta 2010, 1803 (2), 333–41. [PubMed: 19914304]
23. Schneider M; Rosam M; Glaser M; Patronov A; Shah H; Back KC; Daake MA; Buchner J; Antes I, BiPPred: Combined sequence- and structure-based prediction of peptide binding to the Hsp70 chaperone BiP. Proteins: Structure, Function, and Bioinformatics 2016, 84 (10), 1390–1407.
24. Goldenberg DP, Native and non-native intermediates in the BPTI folding pathway. Trends Biochem Sci 1992, 17 (7), 257–61. [PubMed: 1380192]
25. Chang JY, Diverse pathways of oxidative folding of disulfide proteins: underlying causes and folding models. Biochemistry 2011, 50 (17), 3414–31. [PubMed: 21410235]
26. O'Dell SD; Day IN, Molecules in focus Insulin-like growth factor II (IGF-II). The international journal of biochemistry & cell biology 1998, 30 (7), 767–771. [PubMed: 9722981]

27. Sato K; Nakano A, Mechanisms of COPII vesicle formation and protein sorting. FEBS Lett 2007, 581 (11), 2076–82. [PubMed: 17316621]
28. Duguay SJ; Jin Y; Stein J; Duguay AN; Gardner P; Steiner DF, Post-translational processing of the insulin-like growth factor-2 precursor analysis of O-glycosylation and endoproteolysis. Journal of Biological Chemistry 1998, 273 (29), 18443–18451.
29. Chang JY; McFarland NC; Swartz JR, Method for refolding insoluble, misfolded insulin-like growth factor-I into an active conformation. Google Patents: 1994.
30. Kim S-O; Lee Y, Enhanced in vitro refolding selectivity of the recombinant human insulin-like growth factor I. Biotechnology techniques 1997, 11 (2), 85–89.
31. Builder S; Hart R; Lester P; Reifsnyder D, Refolding of polypeptides like recombinant insulin-like growth factor IGF-I. Google Patents: 1998.
32. Brangwynne Clifford P.; Tompa P; Pappu Rohit V., Polymer physics of intracellular phase transitions. Nature Physics 2015, 11 (11), 899–904.
33. Tompa P; Schad E; Tantos A; Kalmar L, Intrinsically disordered proteins: emerging interaction specialists. Curr Opin Struct Biol 2015, 35, 49–59. [PubMed: 26402567]
34. Uversky VN, Protein intrinsic disorder-based liquid-liquid phase transitions in biological systems: Complex coacervates and membrane-less organelles. Adv Colloid Interface Sci 2017, 239, 97–114. [PubMed: 27291647]
35. Banani SF; Lee HO; Hyman AA; Rosen MK, Biomolecular condensates: organizers of cellular biochemistry. Nature Reviews Molecular Cell Biology 2017, 18 (5), 285–298. [PubMed: 28225081]
36. Snead WT; Gladfelter AS, The Control Centers of Biomolecular Phase Separation: How Membrane Surfaces, PTMs, and Active Processes Regulate Condensation. Molecular Cell 2019, 76 (2), 295–305. [PubMed: 31604601]
37. Léger C, Chapter 8 - An Introduction to Electrochemical Methods for the Functional Analysis of Metalloproteins. In Practical Approaches to Biological Inorganic Chemistry, Crichton RR; Louro RO, Eds. Elsevier: Oxford, 2013; pp 179–216.
38. Boeynaems S; Holehouse AS; Weinhardt V; Kovacs D; Van Lindt J; Larabell C; Van Den Bosch L; Das R; Tompa PS; Pappu RV; Gitler AD, Spontaneous driving forces give rise to protein–RNA condensates with coexisting phases and complex material properties. Proceedings of the National Academy of Sciences 2019, 116 (16), 7889.
39. Vacic V; Uversky VN; Dunker AK; Lonardi S, Composition Profiler: a tool for discovery and visualization of amino acid composition differences. BMC Bioinformatics 2007, 8 (1), 211. [PubMed: 17578581]
40. Warwicker J; Charonis S; Curtis RA, Lysine and Arginine Content of Proteins: Computational Analysis Suggests a New Tool for Solubility Design. Molecular Pharmaceutics 2014, 11 (1), 294–303. [PubMed: 24283752]
41. Martin N, Dynamic Synthetic Cells Based on Liquid–Liquid Phase Separation. ChemBioChem 2019, 20 (20), 2553–2568. [PubMed: 31039282]
42. Jakob U; Lilie H; Meyer I; Buchner J, Transient interaction of Hsp90 with early unfolding intermediates of citrate synthase. Implications for heat shock in vivo. J Biol Chem 1995, 270 (13), 7288–94. [PubMed: 7706269]
43. Karagöz GE; Rüdiger SG, Hsp90 interaction with clients. Trends Biochem Sci 2015, 40 (2), 117–25. [PubMed: 25579468]
44. Rudiger S; Freund SM; Veprintsev DB; Fersht AR, CRINEPT-TROSY NMR reveals p53 core domain bound in an unfolded form to the chaperone Hsp90. Proc Natl Acad Sci U S A 2002, 99 (17), 11085–90. [PubMed: 12163643]
45. Hagn F; Lagleder S; Retzlaff M; Rohrberg J; Demmer O; Richter K; Buchner J; Kessler H, Structural analysis of the interaction between Hsp90 and the tumor suppressor protein p53. Nat Struct Mol Biol 2011, 18 (10), 1086–93. [PubMed: 21892170]
46. Park SJ; Borin BN; Martinez-Yamout MA; Dyson HJ, The client protein p53 adopts a molten globule-like state in the presence of Hsp90. Nat Struct Mol Biol 2011, 18 (5), 537–41. [PubMed: 21460846]

47. Melnick J; Dul JL; Argon Y, Sequential interaction of the chaperones BiP and GRP94 with immunoglobulin chains in the endoplasmic reticulum. Nature 1994, 370 (6488), 373–375. [PubMed: 7913987]
48. Sun M; Kotler JLM; Liu S; Street TO, The endoplasmic reticulum (ER) chaperones BiP and Grp94 selectively associate when BiP is in the ADP conformation. J Biol Chem 2019, 294 (16), 6387–6396. [PubMed: 30787103]
49. Banani SF; Lee HO; Hyman AA; Rosen MK, Biomolecular condensates: organizers of cellular biochemistry. Nat Rev Mol Cell Biol 2017, 18 (5), 285–298. [PubMed: 28225081]
50. Boeynaems S; Alberti S; Fawzi NL; Mittag T; Polymenidou M; Rousseau F; Schymkowitz J; Shorter J; Wolozin B; Van Den Bosch L; Tompa P; Fuxreiter M, Protein Phase Separation: A New Phase in Cell Biology. Trends Cell Biol 2018, 28 (6), 420–435. [PubMed: 29602697]
51. Schuster BS; Reed EH; Parthasarathy R; Jahnke CN; Caldwell RM; Bermudez JG; Ramage H; Good MC; Hammer DA, Controllable protein phase separation and modular recruitment to form responsive membraneless organelles. Nat Commun 2018, 9 (1), 2985. [PubMed: 30061688]
52. Woodruff JB; Hyman AA; Boke E, Organization and Function of Non-dynamic Biomolecular Condensates. Trends Biochem Sci 2018, 43 (2), 81–94. [PubMed: 29258725]
53. Lorenson MY; Patel T; Liu JW; Walker AM, Prolactin (PRL) is a zinc-binding protein. I. Zinc interactions with monomeric PRL and divalent cation protection of intragranular PRL cysteine thiols. Endocrinology 1996, 137 (3), 809–16. [PubMed: 8603589]
54. Baumann GP, Growth hormone isoforms. Growth hormone & IGF research : official journal of the Growth Hormone Research Society and the International IGF Research Society 2009, 19 (4), 333–40.
55. Noormägi A; Gavrilova J; Smirnova J; Tõugu V; Palumaa P, Zn(II) ions co-secreted with insulin suppress inherent amyloidogenic properties of monomeric insulin. The Biochemical journal 2010, 430 (3), 511–8. [PubMed: 20632994]
56. Erthal LC; Marques AF; Almeida FC; Melo GL; Carvalho CM; Palmieri LC; Cabral KM; Fontes GN; Lima LM, Regulation of the assembly and amyloid aggregation of murine amylin by zinc. Biophysical chemistry 2016, 218, 58–70. [PubMed: 27693831]
57. Huard DJE; Jonke AP; Torres MP; Lieberman RL, Different Grp94 components interact transiently with the myocilin olfactomedin domain in vitro to enhance or retard its amyloid aggregation. Sci Rep 2019, 9 (1), 12769. [PubMed: 31484937]
58. Weickert S; Wawrzyniuk M; John LH; Rudiger SGD; Drescher M, The mechanism of Hsp90-induced oligomerizaton of Tau. Sci Adv 2020, 6 (11), eaax6999. [PubMed: 32201713]
59. Huang B; Friedman LJ; Sun M; Gelles J; Street TO, Conformational Cycling within the Closed State of Grp94, an Hsp90-Family Chaperone. Journal of Molecular Biology 2019, 431 (17), 3312–3323. [PubMed: 31202885]
60. Huck JD; Que NL; Hong F; Li Z; Gewirth DT, Structural and Functional Analysis of GRP94 in the Closed State Reveals an Essential Role for the Pre-N Domain and a Potential Client-Binding Site. Cell Rep 2017, 20 (12), 2800–2809. [PubMed: 28930677]
61. Krukenberg KA; Bottcher UM; Southworth DR; Agard DA, Grp94, the endoplasmic reticulum Hsp90, has a similar solution conformation to cytosolic Hsp90 in the absence of nucleotide. Protein science : a publication of the Protein Society 2009, 18 (9), 1815–27. [PubMed: 19554567]
62. Dollins DE; Warren JJ; Immormino RM; Gewirth DT, Structures of GRP94-nucleotide complexes reveal mechanistic differences between the hsp90 chaperones. Molecular cell 2007, 28 (1), 41–56. [PubMed: 17936703]
63. Krukenberg KA; Böttcher UMK; Southworth DR; Agard DA, Grp94, the endoplasmic reticulum Hsp90, has a similar solution conformation to cytosolic Hsp90 in the absence of nucleotide. Protein Science 2009, 18 (9), 1815–1827. [PubMed: 19554567]
64. Wisniewska M; Karlberg T; Lehtio L; Johansson I; Kotenyova T; Moche M; Schuler H, Crystal structures of the ATPase domains of four human Hsp70 isoforms: HSPA1L/Hsp70-hom, HSPA2/Hsp70–2, HSPA6/Hsp70B', and HSPA5/BiP/GRP78. PLoS One 2010, 5 (1), e8625. [PubMed: 20072699]

65. Lavery LA; Partridge JR; Ramelot TA; Elnatan D; Kennedy MA; Agard DA, Structural asymmetry in the closed state of mitochondrial Hsp90 (TRAP1) supports a two-step ATP hydrolysis mechanism. Mol Cell 2014, 53 (2), 330–43. [PubMed: 24462206]

66. Stetefeld J; McKenna SA; Patel TR, Dynamic light scattering: a practical guide and applications in biomedical sciences. Biophys Rev 2016, 8 (4), 409–427. [PubMed: 28510011]

67. Friedman LJ; Chung J; Gelles J, Viewing dynamic assembly of molecular complexes by multi-wavelength single-molecule fluorescence. Biophys J 2006, 91 (3), 1023–31. [PubMed: 16698779]

68. Huang B; Friedman LJ; Sun M; Gelles J; Street TO, Conformational Cycling within the Closed State of Grp94, an Hsp90-Family Chaperone. J Mol Biol 2019, 431 (17), 3312–3323. [PubMed: 31202885]

69. Friedman LJ; Gelles J, Multi-wavelength single-molecule fluorescence analysis of transcription mechanisms. Methods 2015, 86, 27–36. [PubMed: 26032816]

Highlights

- ProIGF2 form oligomers and E-peptide region is responsible for oligomerization.
- Bip and Grp94 exert counteracting effects on proIGF2 oligomerization.
- Grp94 enhances proIGF2 oligomerization by interacting with dynamic oligomers.
- Bip and Grp94 only moderately slow down proIGF2 folding by stabilizing the unfolded state.

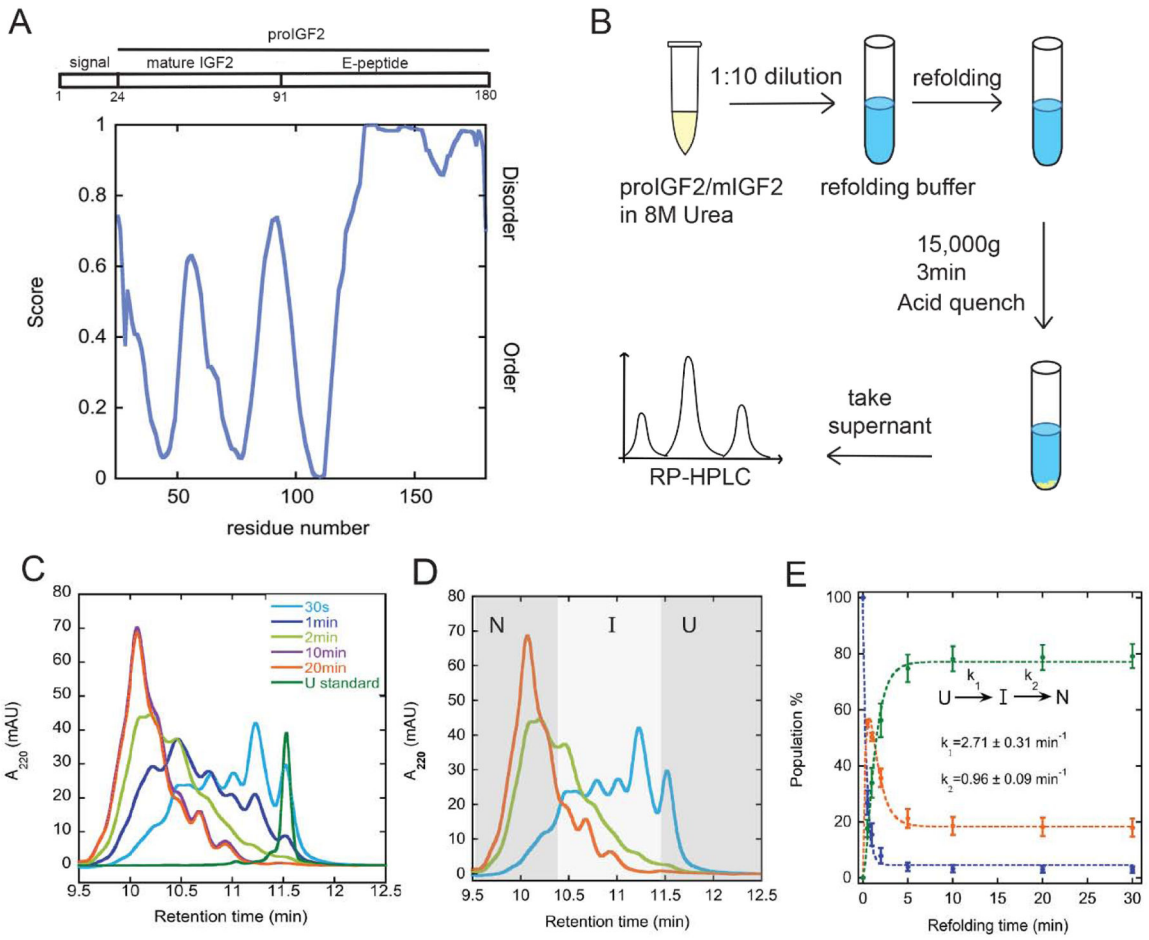

Figure 1.

ProIGF2 oxidative protein folding. **(A)** The proIGF2 E-peptide is an intrinsically disordered region. Disorder prediction of proIGF2 is calculated with PONDR-VLXT[69]. **(B)** Protocol to populate and characterize proIGF2 folding states by RP-HPLC. **(C)** HPLC chromatograms of proIGF2 folding intermediates quenched at various folding times. Folding times shown in the legend. The fully reduced peak elutes at 11.5min (U standard), whereas the oxidized populations elute at earlier times. **(D)** ProIGF2 folding is categorized into three states (U, I, and N). **(E)** Populations of proIGF2 were fitted with a three-state model (see Methods). The populations of U, I and N are color-coded in blue, orange, and green respectively. Error bars are the S.E.M of at least three measurements. Refolding buffer: 50mM Tris pH 7.5, 100mM KCl, 1mM ATP, 1mM $MgCl_2$, 1.25mM GSSG, 6.25 mM GSH, 0.8M urea, 37°C.

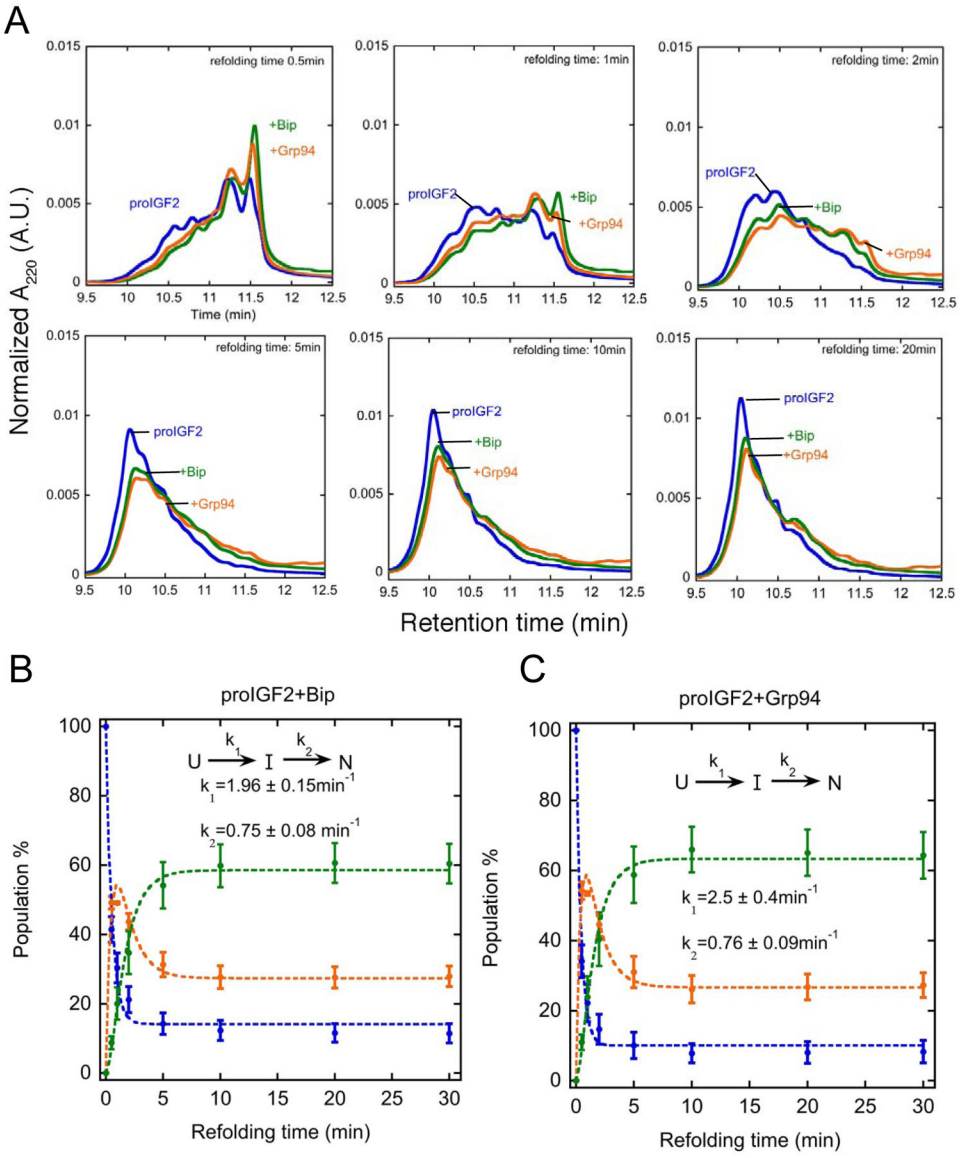

Figure 2.

A) Influence of BiP and Grp94 on the folding of proIGF2. HPLC elution profiles of proIGF2 with and without chaperone are compared at various refolding times. Peak areas are normalized for a direct comparison between different conditions. Refolding buffer conditions are the same as Figure 1. Populations of proIGF2 in the presence of Bip **(B)** and Grp94 **(C)** were fitted with a three-state model as Figure 1E. The populations of U, I and N are color-coded in blue, orange, and green respectively. Error bars are the S.E.M of at least three measurements. Refolding buffer: 50mM Tris pH 7.5, 100mM KCl, 1mM ATP, 1mM $MgCl_2$, 1.25mM GSSG, 6.25 mM GSH, 0.8M urea, 37°C.

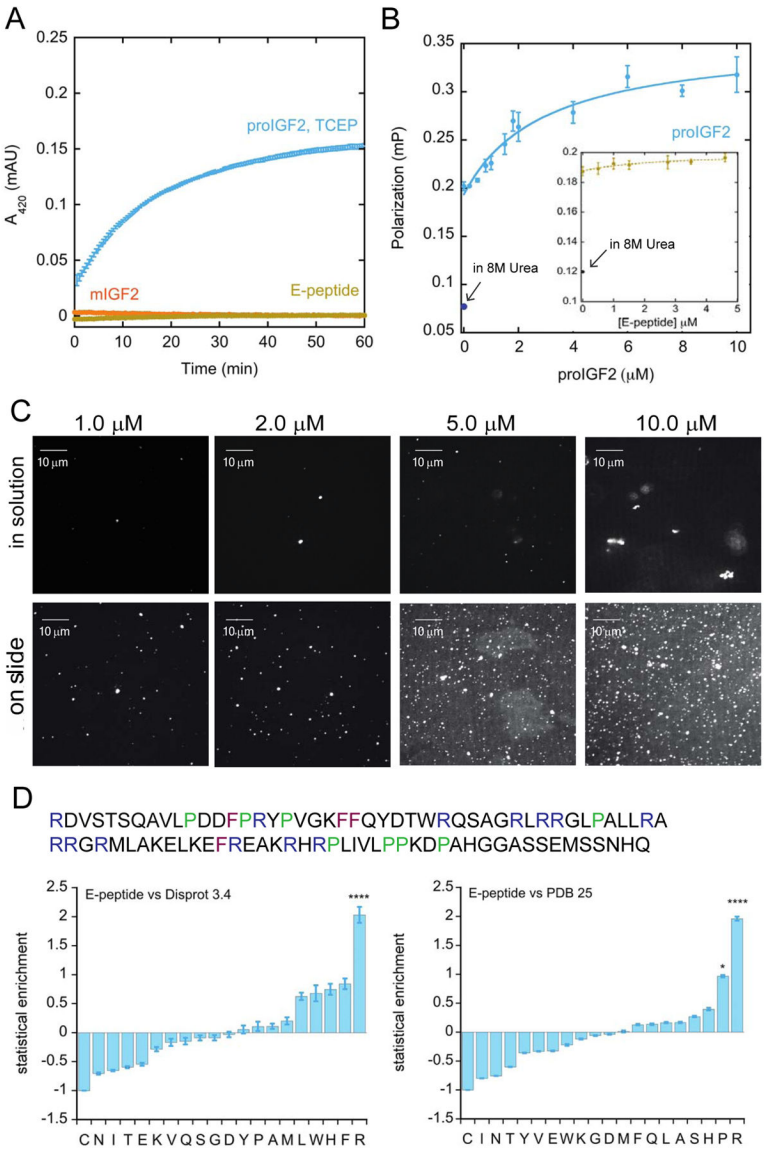

Figure 3.

A) ProIGF2 produces light scattering under reducing conditions (TCEP), as measured by increased light absorption at 420 nm. Solid line is a single exponential fit (0.057 ± 0.003 min $^{-1}$). Error bars are the S.E.M of at least three measurements. **B)** FITC-labeled proIGF2 and E-peptide (inset) were titrated with corresponding unlabeled constructs under TCEP conditions. Solid line is a single site binding model fit (ProIGF2 $K_{d,app}$ = 2.98 ± 0.66 μM; E-peptide $K_{d,app}$ = 2.5 ± 2.1μM, uncertainty from fitting error). Monomeric proIGF2 and E-peptide (in 8M urea) has a low fluorescence depolariztion value. Error bars are the S.E.M of at least three measurements. **C)** Images of Alexa 647-labeled proIGF2 oligomers visualized by confocal microscopy. **D)** E-peptide composition analysis. Upper: E-peptide amino acid sequence. Phenylalanine, Proline and Arginine are color-coded in purple, green and blue respectively. Lower: E-peptide amino acid composition comparison to DisProt 3.4 and PDB select 25 calculated with Composition Profiler (http://www.cprofiler.org,[38] * P ≤ 0.05; ****

$P \leq 0.0001$ calculated via t-test). Y-axis statistical enrichment (h_k) is the residue probability differences between E-peptide (p_k) and the background sample from bootstrap sampling (q_k), where $h_k = \frac{p_k - q_k}{q_k}$. DisProt 3.4 is a set of experimentally determined disordered protein, and the PDB select 25 is a subset of structures from Protein Data Bank (PDB) with less than 25% sequence identity. Error bars are the standard deviations of the observed statistical enrichment (h_k) of 10,000 times bootstrap sampling.

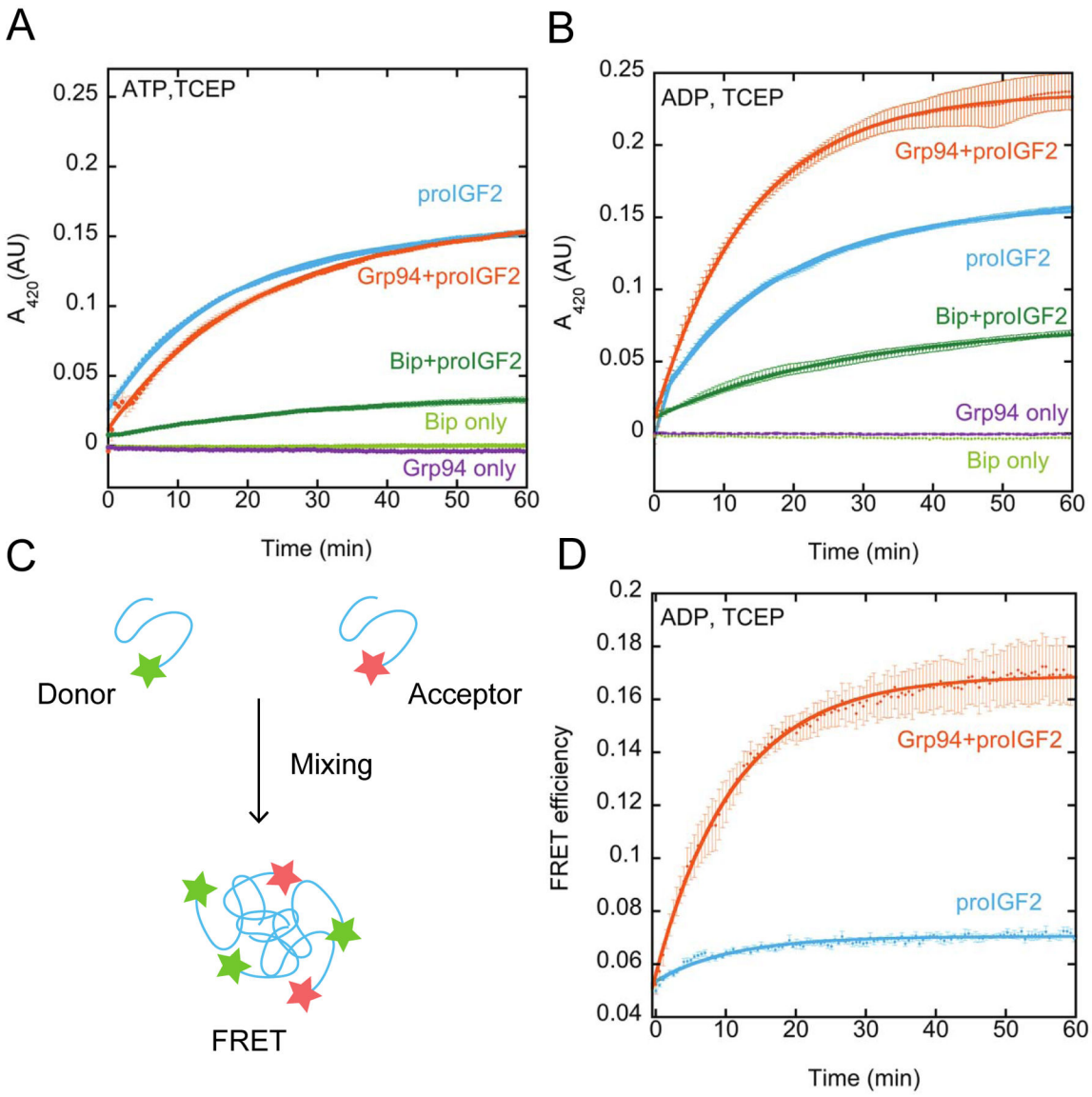

Figure 4.

A&B) ProIGF2 light scattering measurements in the presence of BiP and Grp94 under ATP and ADP conditions. Solid lines are single exponential fits (proIGF2 ATP conditions: 0.057 ± 0.003 min^{-1}; proIGF2 and Grp94 ATP conditions: 0.045 ± 0.001 min^{-1}; proIGF2 ADP conditions: 0.052 ± 0.001 min^{-1}; proIGF2 and Grp94 ADP conditions: 0.074 ± 0.008 min^{-1}). **C)** Design of proIGF2 oligomerization FRET measurement. **D)** ProIGF2 FRET in the absense and presence of Grp94 under ADP conditions. Solid line is a single exponential fit (proIGF2 and Grp94: 0.10± 0.01 min^{-1}, proIGF2: 0.12± 0.04 min^{-1}). Error bars are the S.E.M of at least three measurements. Buffer conditions: 50mM Tris pH 7.5, 100mM KCl, 1mM ATP /1mM ADP, 1mM $MgCl_2$, 5mM TCEP, 0.8M urea. Error bars are the S.E.M of at least three measurements.

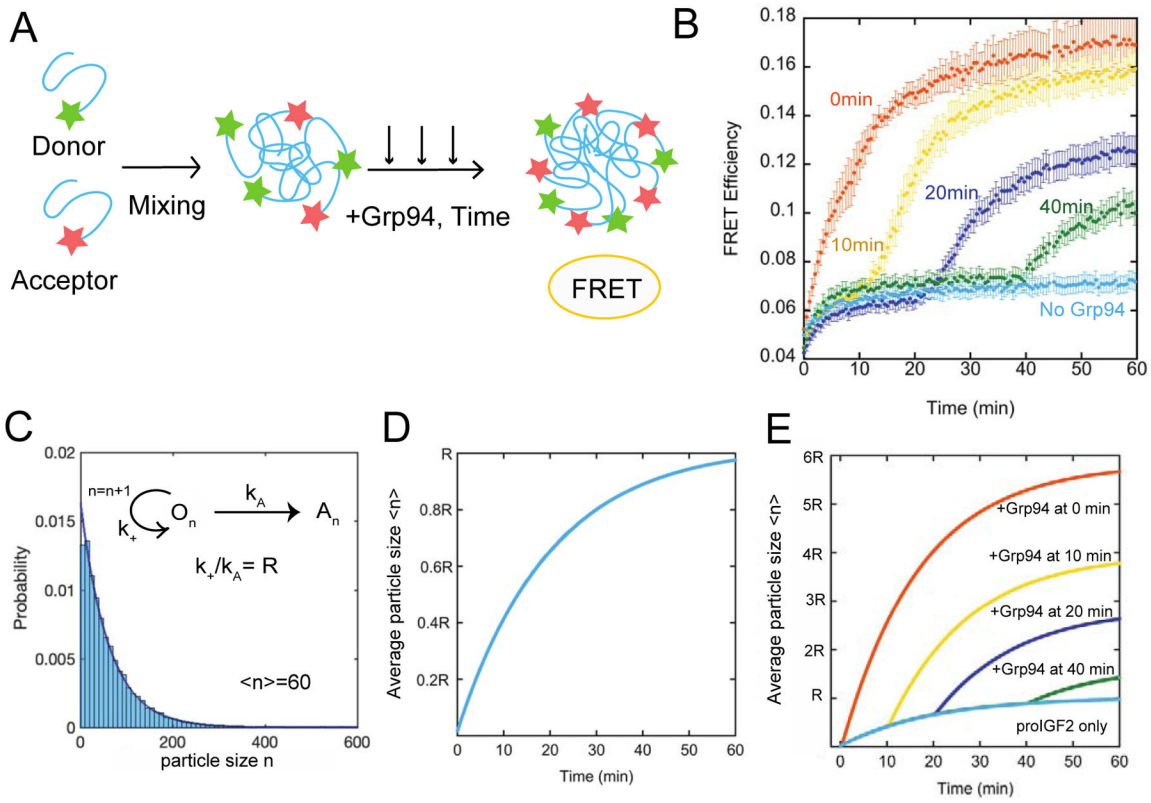

Figure 5.

A) Design of proIGF2 oligomerization FRET measurement with Grp94 introduced to proIGF2 oligomers at variable times. **B)** ProIGF2 FRET in the absence and presence of Grp94 under ADP conditions. Error bars are the S.E.M of at least three measurements. Buffer conditions are the same as Figure 4D. **C)** ProIGF2 aggregation and oligomerization model and numerical simulation. Monomers are added to oligomers with a rate of k_+ while oligomers transition to aggregates with a rate of k_A. Numerical simulation of proIGF2 particle size distribution with k_A=0.05min^{-1}, k_+=3min^{-1} after one hour of oligomer growth. Solid line is a single exponential fit. **D)** Numerical simulation of proIGF2 particle growth over time with k_A=0.05min^{-1}and k_+=3min^{-1}. **E)** Numerical simulations of proIGF2 oligomerization with Grp94 introduced at various times to match the FRET measurements in Figure 5B. The k_+ is increased 6-fold by Grp94, therefore the maximium average oligomer size <n> is 6R.

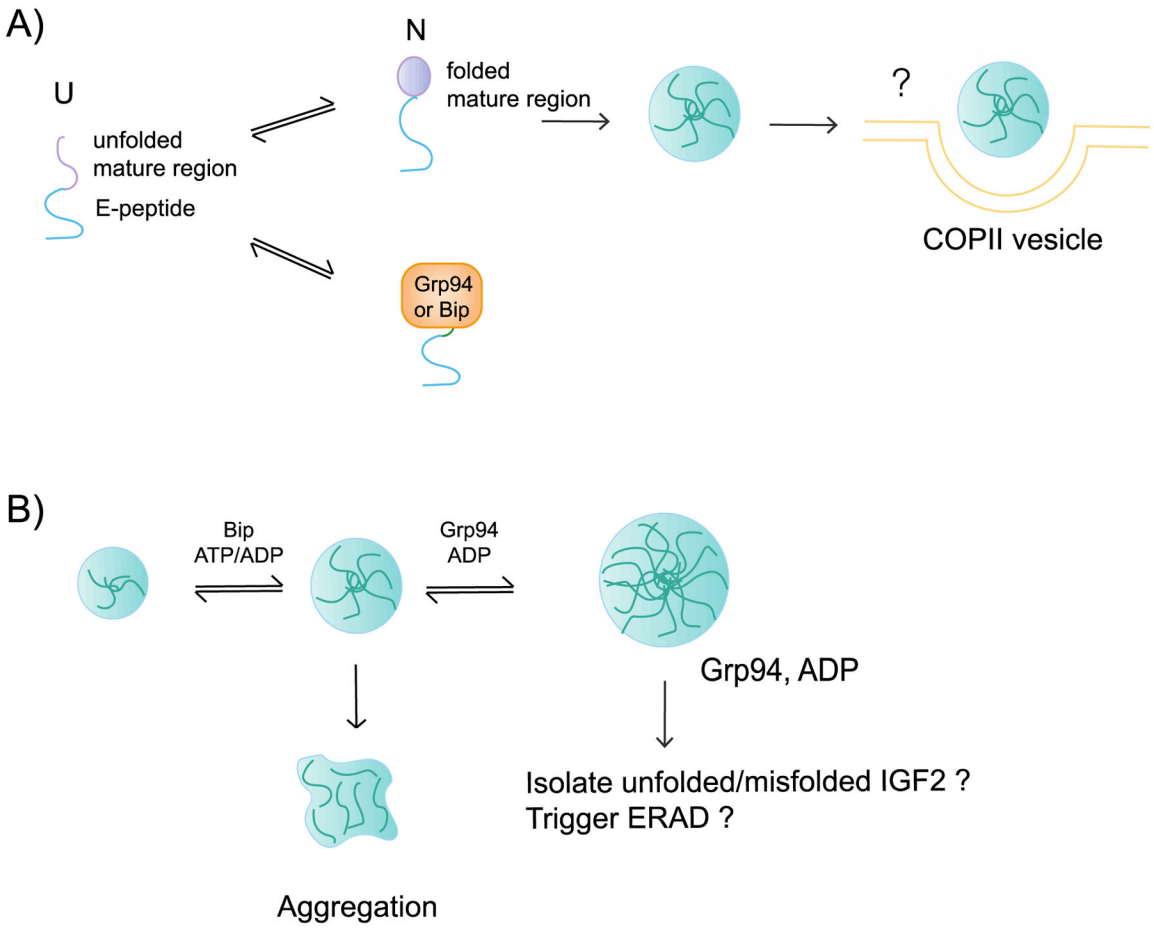

Figure 6.

Schematic illustration of Grp94 and BiP chaperone influence on proIGF2. **A)** Both BiP and Grp94 stabilize unfolded proIGF2. The E-peptide region promotes proIGF2 oligomerization, potentially facilitating the packaging of proIGF2 into vesicles for transportation to Golgi. **B)** Grp94 in the open conformation (ADP) binds to proIGF2 oligomers and increases their size. BiP decreases the size of proIGF2 oligomers. Regulated proIGF2 oligomerization may trigger the ER-associated degradation pathway or be a mechanism to isolate unfolded and misfolded species of proIGF2.

Table 1.

ProIGF2 average particle size (R_H) measured by DLS.

Measurements were taken directly after oligomer formation (0 hr) and after 1 hour of incubation in the reaction buffer: 50mM Tris pH 7.5, 100mM KCl, 1mM ATP, 1mM $MgCl_2$, 5mM TCEP, 0.8M urea.

	0 hr (nm)	1 hr (nm)
ProIGF2	230	747
ProIGF2+Bip	274	67
ProIGF2+Grp94	311	1370